Article

Entangled Dual Universe

Mohammed B. Al-Fadhli [1,*]

[1] College of Science, University of Lincoln, Lincoln, LN6 7TS, UK.
* Correspondence: malfadhli@lincoln.ac.uk; mo.fadhli7@gmail.com.

Abstract: Advances in cosmology and astronomical observations over the last two decades have revealed significant tensions and many ambiguities within the standard model of cosmology of a spatially flat Universe, the lambda cold dark matter model. Moreover, the recent Planck Legacy 2018 (PL18) release has confirmed the presence of an enhanced lensing amplitude in the cosmic microwave background (CMB) power spectra, which prefers a positively curved early Universe with a confidence level higher than 99%. This paper addresses the study of a quantum mechanism that could replace the concept of dark matter and energy by considering a primordial curvature as preferred by the PL18 release while yielding the present-day spatial flatness. The implied primordial curvature is incorporated as the background curvature to extend the field equations in terms of the brane-world modified gravity. The Universe evolution is modelled by utilizing a new wavefunction of the Universe that propagates in the bulk with reference to the scale factor of the early Universe and its radius of curvature upon the emission of the CMB, which revealed both positive and negative solutions. This characteristic implies that a pair of entangled wavefunctions was created and evolved in opposite directions as a manifestation of distinct matter and antimatter sides of the Universe. The wavefunction indicates a nascent hyperbolic expansion away from early energy is followed by a first phase of decelerating expansion during the first ~10 Gyr, and then, a second phase of accelerating expansion in reverse directions, whereby both sides free-fall towards each other under gravitational acceleration. The predicted background curvature evolution demonstrates the fast orbital speed of outer stars owing to external fields exerted on galaxies as they travelled through earlier conformally curved spacetime. Finally, the wavefunction predicts an eventual phase of rapid spatial contraction that culminates in a Big Crunch, signaling a cyclic Universe. These findings reveal that early plasma could be separated and evolved into distinct sides of the Universe that collectively and geometrically inducing its evolution, physically explaining the effects attributed to dark matter and energy.

Keywords: Duality; Antimatter; Brane-World Modified Gravity.

1. Introduction

The Planck Collaboration released in 2018 the most thorough spectrum of the cosmic microwave background (CMB), the first light in the Universe. The Planck Legacy 2018 (PL18) release has confirmed the presence of an enhanced lensing amplitude in the CMB power spectra, which prefers a positively curved early Universe with a confidence level higher than 99% [1,2]. Although the spatial flatness could be recovered by combining the CMB lensing and baryon acoustic oscillation (BAO) data, concerns were raised regarding the reliability of this combination because the curvature parameter tension between these sets of data was measured to be 2.5 to 3σ [3]. In contrast, the closed Universe can naturally elucidate the anomalous lensing amplitude, aid a large-scale cut-off in primaeval density fluctuations [1] and agree with low CMB anisotropy observations [4,5].

Despite the successes of the lambda cold dark matter model, it masks large areas of ambiguity [6]. It was built based on unclear ingredients, namely, inflation, dark matter and energy, which have not been identified or fully understood despite extensive research efforts over decades [7–9]. It leaves numerous enigmas including the inferred baryon asymmetry, the fine tuning and coincidence problems, etc [10–12]. Moreover, advances in cosmology and enhanced accuracy of observations have revealed inconsistencies among key parameters of the model; notably, the Hubble tension at 4 to 6σ [13,14].

Preprints (www.preprints.org) | NOT PEER-REVIEWED | Posted: 29 December 2022 doi:10.20944/preprints202005.0250.v11

This paper addresses the study of a quantum mechanism that could replace the concept of dark matter and energy by considering a primordial curvature as preferred by the PL18 release while yielding a present-day spatial flatness. The primordial curvature and its evolution over the conformal time is incorporated to extend the field equations in terms of brane-world modified gravity in order to approach the problems of accelerated expansion and fast orbital speed of outer stars from a new perspective. This paper is organised as follows. Section 2 presents extended field equations, Sections 3 and 4 discuss the Universe model and its evolution. Section 5 presents spiral galaxy formation and rotation. Section 6 discusses the Universe minimal radius. Finally, Section 7 concludes this work and suggests future works.

2. Field Equations for Conformally Curved Spacetime

The recent PL18 release has preferred a positively curved early Universe, that is, is a sign of a background curvature or a curved bulk. To incorporate the bulk curvature and its evolution over conformal time, a modulus of spacetime deformation, E_D, is introduced based on the theory of elasticity [15]. The modulus can be expressed in terms of the bulk resistance to the localized curvature that is induced by celestial objects by using Einstein field equations or in terms of the bulk field strength by using the Lagrangian formulation of the energy density exists in the bulk as a manifestation of vacuum energy density as

$$E_D = \frac{T_{\mu\nu} - T g_{\mu\nu}/2}{R_{\mu\nu}/\mathcal{R}} = \frac{-\mathcal{F}_{\lambda\rho}\mathcal{F}^{\lambda\rho}}{4\mu_0} \tag{1}$$

where the stress-energy tensor $T_{\mu\nu}$ of trace T signifies the stress while the strain is signified by Ricci curvature tensor $R_{\mu\nu}$ as the change in the curvature divided by the scalar of the bulk curvature $\mathcal{R}$. $\mathcal{F}_{\lambda\rho}$ is the field strength tensor and μ_0 is vacuum permeability. By incorporating the bulk influence, the Einstein–Hilbert action can be extended to

$$S = E_D \int \left[\frac{R_{\mu\nu}g^{\mu\nu}}{\mathcal{R}_{\mu\nu}\tilde{g}^{\mu\nu}} + \frac{L_{\mu\nu}g^{\mu\nu}}{\mathcal{L}_{\mu\nu}\tilde{g}^{\mu\nu}}\right]\sqrt{-g}\, d^4\rho \tag{2}$$

As the modulus, E_D, is constant with regards to the cloud-world action under the constant vacuum energy density condition, and by considering the expansion of the bulk over the conformal time owing to the Universe expansion (scale factor evolution) and its implication on the field strength of the bulk, a dual-action concerning the conservation of energy on global (bulk) and local (cloud-world) scales can be introduced as

$$S = \int_B \left[\frac{-\mathcal{F}_{\lambda\rho}\tilde{g}^{\lambda\gamma}\mathcal{F}_{\gamma\alpha}\tilde{g}^{\rho\alpha}}{4\mu_0}\right]\sqrt{-\tilde{g}} \int_C \left[\frac{R_{\mu\nu}g^{\mu\nu}}{\mathcal{R}_{\mu\nu}\tilde{g}^{\mu\nu}} + \frac{L_{\mu\nu}g^{\mu\nu}}{\mathcal{L}_{\mu\nu}\tilde{g}^{\mu\nu}}\right]\sqrt{-g}\, d^4\rho\, d^4\sigma \tag{3}$$

where $R_{\mu\nu}$ is Ricci curvature tensor representing the localized curvature induced in the bulk by a celestial object that is regarded as a 4D relativistic cloud-world of metric g_{uv} and Lagrangian density $L_{\mu\nu}$ whereas $\mathcal{R}_{\mu\nu}$ is the curvature tensor of 4D bulk of metric $\tilde{g}_{\mu\nu}$ and Lagrangian density $\mathcal{L}_{\mu\nu}$ as its internal stresses and momenta reflecting its curvature. The action can be further extended in terms of quantum wave interactions as follows

$$S = \int_B \left[\frac{-\mathcal{F}_{\lambda\rho}\tilde{g}^{\lambda\gamma}\mathcal{F}_{\gamma\alpha}\tilde{g}^{\rho\alpha}}{4\mu_0}\right]\sqrt{-\tilde{g}} \int_C \left[\frac{R_{\mu\nu}g^{\mu\nu}}{\mathcal{R}_{\mu\nu}\tilde{g}^{\mu\nu}}\right]\sqrt{-g} \int_Q \left[\frac{p_\mu p_\nu q^{\mu\nu}}{\pi_\mu\pi_\nu g^{\mu\nu}} + \frac{L_{\alpha\beta}q^{\alpha\lambda}L_{\lambda\gamma}q^{\beta\gamma}}{n\mathcal{L}_{\mu\nu}g^{\mu\nu}}\right]\sqrt{-q}\, \vartheta^2 d^{12}\rho \tag{4}$$

where $L_{\alpha\beta}L^{\alpha\beta}$ are Lagrangian densities of two entangled quantum fields of a metric $q_{\mu\nu}$ and four-momentum $p_\mu p^\nu$ whereas $\pi_\mu\pi^\nu$ are the four-momentum of vacuum energy density of a Lagrangian density $\mathcal{L}_{\mu\nu}g^{\mu\nu}$, ϑ^2 is a dimensional-hierarchy factor and n is a proportionality constant.

Preprints (www.preprints.org) | NOT PEER-REVIEWED | Posted: 29 December 2022 doi:10.20944/preprints202005.0250.v11

By applying the principle of stationary action for the Equation (3) in [16] yields

$$\frac{R_{\mu\nu}}{\mathcal{R}} - \frac{1}{2}\frac{R}{\mathcal{R}}g_{\mu\nu} - \frac{R\mathcal{R}_{\mu\nu}}{\mathcal{R}^2} + \frac{R(\mathcal{K}_{\mu\nu} - \frac{1}{2}\mathcal{K}\hat{q}_{\mu\nu}) - \mathcal{R}(K_{\mu\nu} - \frac{1}{2}K\hat{q}_{\mu\nu})}{\mathcal{R}^2} = \frac{\hat{T}_{\mu\nu}}{\mathcal{T}_{\mu\nu}} \tag{5}$$

As visualized in Section 5, these field equations can be interpreted as describing the flow and interaction of a 4D relativistic cloud-world of intrinsic $R_{\mu\nu}$ and extrinsic $K_{\mu\nu}$ curvatures and the 4D conformal bulk of intrinsic $\mathcal{R}_{\mu\nu}$ and extrinsic $\mathcal{K}_{\mu\nu}$ curvatures. The equations can indicate that the induced curvature, R, of the cloud-world over the bulk background (existing) curvature, $\mathcal{R}$, equals the ratio of the cloud-world imposed energy density and its flux, $\hat{T}_{\mu\nu}$, to the bulk vacuum energy density and its flux, $\mathcal{T}_{\mu\nu}$, throughout the expanding/contracting Universe. Because $\mathcal{R}_{\mu\nu}/\mathcal{R} = \mathcal{R}_{\mu\nu}/\mathcal{R}_{\mu\nu}\tilde{g}^{\mu\nu} = \tilde{g}_{\mu\nu}$, which reflects the bulk intrinsic curvature, and by transforming the boundary term of the bulk as in [16], comparing Equation (1) with Einstein field equations and then substituting to Equations (5), the field equations can be simplified to

$$R_{\mu\nu} - \frac{1}{2}R\hat{g}_{\mu\nu} - (K_{\mu\nu} - \frac{1}{2}K\hat{q}_{\mu\nu}) = \frac{8\pi G_{\mathcal{R}}}{c^4}\hat{T}_{\mu\nu} \tag{6}$$

where $\hat{g}_{\mu\nu} = g_{\mu\nu} + 2\tilde{g}_{\mu\nu} + 2\bar{\tilde{g}}_{\mu\nu}$ is the conformally transformed metric tensor counting for the contributions of the cloud-world metric, $g_{\mu\nu}$, in addition to the contribution from the intrinsic and extrinsic curvatures of the bulk based on $\tilde{g}_{\mu\nu}$ and $\bar{\tilde{g}}_{\mu\nu}$ respectively. The effective Newtonian parameter $G_{\mathcal{R}}$ reflect the bulk curvature and can accommodate its evolution over the conformal time against constant G for a special flat spacetime case. $\hat{T}_{\mu\nu} \coloneqq (2L_{\mu\nu} - L\hat{g}_{\mu\nu}) - (2l_{\mu\nu} - l\hat{q}_{\mu\nu})$ is an extended conformal stress-energy tensor that is defined by including the Lagrangian density of the energy density and flux of the cloud-world, $L_{\mu\nu}$, and the electromagnetic energy flux from its boundary, $l_{\mu\nu}$, over conformal time whereas the term $(K_{\mu\nu} - K\hat{q}_{\mu\nu}/2)$ represents the corresponding extrinsic curvature of the cloud-world's boundary. The field equations could remove the singularities and satisfy a conformal invariance theory. In addition, by applying the principle of stationary action for Equation (4) in [16], the equations in terms of quantum wave interactions are

$$\hat{p}_\mu - \frac{1}{2}\hat{p}^\nu\xi_{\mu\nu} - (J^\mu A_\mu - \frac{1}{2}J^\mu A^\nu\zeta_{\mu\nu}) = \frac{1}{2}\frac{\hbar G_{\mathcal{R}}}{c^2 g_R}\hat{\mathcal{T}}_\mu \tag{7}$$

where $\hat{p}_\mu$ is the momentum operator, $\hat{\mathcal{T}}_\mu$ is the stress-energy (gravitational) operator and $\xi_{\mu\nu} = q_{\mu\nu} + 2\tilde{q}_{\mu\nu} + 2\bar{\tilde{q}}_{\mu\nu}$ is the conformally transformed metric tensor counting for the contributions of the quantum cloud's metric, $q_{\mu\nu}$, in addition to the contribution from the intrinsic and extrinsic curvatures of the parent-world given by $\tilde{q}_{\mu\nu}$ and $\bar{\tilde{q}}_{\mu\nu}$ metrics, respectively. Accordingly, the quantized field equations are

$$i\hbar\gamma^\mu\partial_\mu\psi - \frac{1}{2}i\hbar\gamma^\mu\partial^\nu\xi_{\mu\nu}\psi - (J^\mu A_\mu - \frac{1}{2}J^\mu A^\nu\zeta_{\mu\nu})\psi = \frac{1}{2}\frac{\hbar}{x^\mu}R\partial_R\psi \tag{8}$$

These field equations reduce to quantum electrodynamics for undeformed configuration of the quantum cloud in a flat spacetime background as presented in [16], where γ^μ are Dirac matrices and $\partial_R\psi$ is part of the gravitational operator based on a plane wavefunction, $\psi = Ae^{-i(\omega t - kx)}$, which can be expressed by utilizing Equation (7) as

$$\psi = A\,exp\frac{-iR^2}{2Mc^2}\,T_\mu x^\mu \tag{9}$$

where T_μ is the stress-energy of the quantum cloud while the gravitational field strength of the parent cloud-world of mass M and at radius R is $g_R = MG_{\mathcal{R}}/R^2$.

Preprints (www.preprints.org) | NOT PEER-REVIEWED | Posted: 29 December 2022 doi:10.20944/preprints202005.0250.v11

3. Early Universe Closed Metric Model

The Friedmann–Lemaître metric is the standard cosmological metric model, which assumes an isotropic and homogenous Universe [17,18], where the isotropy and homogeneity of early Universe plasma based on the CMB are consistent with this metric. The PL18 preferred a closed early Universe; thus, the plasma reference radius of curvature r_P upon the emission of the CMB and the corresponding early Universe scale factor a_P at the reference cosmic time t_p are incorporated to reference this metric shown in Figure 1.

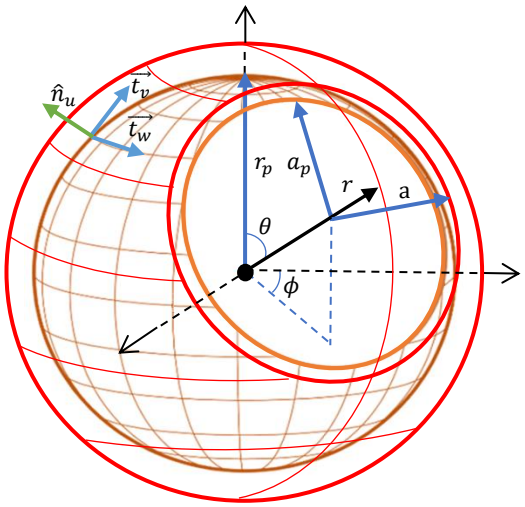

Figure 1. The hypersphere of a positively curved early Universe plasma upon the CMB emissions. r_p is the reference radius of the intrinsic curvature and a_p is the reference scale factor of the early Universe. $\hat{n}_u$ and $\vec{t}_v$ are the normal and tangential vectors on the manifold boundary respectively regarding the extrinsic curvature.

The four-dimension spacetime interval of the referenced metric tensor $g_{\mu\nu}$ is

$$ds^2 = c^2\,dt^2 - \frac{a^2}{{a_p}^2}\left(\frac{dr^2}{1-\frac{r^2}{{r_p}^2}} + r^2\,d\theta^2 + r^2 sin^2\theta\,d\phi^2\right) \tag{10}$$

where a/a_p is a new dimensionless scale factor. At the reference imaginary time τ_p, there is no conformal distortion yet, i.e., the global and local boundaries are the same. By using Christoffel symbols of the second kind for g_{uv} in Equation (10), the Ricci curvature tensor and scalar are (derivations in Appendix A):

$$\begin{aligned} R_{tt} &= -3\frac{\ddot{a}}{a}, \qquad R_{rr} = \frac{1}{c^2}\left(\frac{a\ddot{a}}{{a_p}^2} + \frac{2\dot{a}^2}{{a_p}^2} + \frac{2c^2}{{r_p}^2}\right)\Big/\left(1-\frac{r^2}{{r_p}^2}\right), \\ R_{\theta\theta} &= \frac{r^2}{c^2}\left(\frac{a\ddot{a}}{{a_p}^2} + \frac{2\dot{a}^2}{{a_p}^2} + \frac{2c^2}{{r_p}^2}\right), \qquad R_{\phi\phi} = \frac{r^2 sin^2\theta}{c^2}\left(\frac{a\ddot{a}}{{a_p}^2} + \frac{2\dot{a}^2}{{a_p}^2} + \frac{2c^2}{{r_p}^2}\right), \end{aligned} \tag{11}$$

The Ricci scalar curvature is

$$R = R_{\mu\nu}\,g^{\mu\nu} = -\frac{6}{c^2}\left(\frac{\ddot{a}}{a} + \frac{\dot{a}^2}{a^2} + \frac{c^2\,{a_p}^2}{a^2\,{r_p}^2}\right). \tag{12}$$

where the dotes are time derivatives.

Preprints (www.preprints.org) | NOT PEER-REVIEWED | Posted: 29 December 2022 doi:10.20944/preprints202005.0250.v11

By solving the field equations for a perfect fluid given by $T_{\mu\nu} = (\rho + P/c^2)\, u_\mu u_\nu + P g_{\mu\nu}$ [19–21] and substituting Equations (10)-(12), the Friedmann equations that count for the plasma reference radius and reference scale factor are

$$H^2 \equiv \frac{\dot{a}^2}{a^2} = \frac{8\pi G_{\mathcal{R}}\rho}{3} - \frac{c^2 {a_p}^2}{a^2 {r_p}^2} \tag{13}$$

$$\dot{H} \equiv \frac{\ddot{a}}{a} = -\frac{4\pi G_{\mathcal{R}}}{3}\left(\rho + 3\frac{P}{c^2}\right) \tag{14}$$

where H, P, and ρ are Hubble parameter, pressure, and density respectively. By utilizing the imaginary cosmic time, $\tau = it$, the referenced Friedman equations can be solved at the reference time τ_p by rewriting Equation (13) in terms of the conformal time in its parametric form, $d\eta = \frac{a_p}{a} dt$ (where $\dot{a} = \frac{da}{dt}$); thus, $d\eta = \frac{a_p}{a\dot{a}} da$:

$$\int_0^\eta d\eta = \int_0^{2\pi} a_p \left(\frac{8\pi G_p \rho_p {a_p}^3}{3} a - \frac{c^2 {a_p}^2}{{r_p}^2} a^2\right)^{-1/2} da \tag{15}$$

where $\rho = \rho_p {a_p}^3 / a^3$ [22]. By integrating, the dimensionless scale factor evolution is

$$\frac{a(\eta)}{a_p} = \frac{G_p M_p}{c^2 r_p}\left(1 - cos\frac{c}{r_p}\eta\right) \tag{16}$$

where $M_p = \frac{4}{3}\pi\, \rho_p {r_p}^3$ is the early Universe plasma mass. The gravitational radius of early Universe is $G_p M_p / c^2$. The amplitude of Equation (16) can be rewritten in terms of early Universe energy density E_p (total energy) and the modulus E_D representing vacuum energy density by using Equations (1) as follows

$$\frac{a(\eta)}{a_p} = \frac{E_p}{6E_D}\left(1 - cos\frac{c}{r_p}\eta\right) \tag{17}$$

Additionally, the evolution of the imaginary cosmic time $\tau(\eta)$ can be obtained by integrating the scale factor over the expansion speed H_η while initiating at the reference imaginary time τ_p with the corresponding spatial scale factor a_p. By rewriting Equation (17) in terms of the Hubble parameter at τ_p as $d\tau = i\frac{da(\eta)}{H a_p}$, gives

$$\int_{\tau_P}^{\tau} d\tau = i\int_0^\eta \frac{E_p}{6H_\eta E_D}\left(1 - cos\frac{c}{r_p}\eta\right) d\eta \tag{18}$$

By performing the integration, the imaginary time evolution is

$$\tau(\eta) = i\frac{E_p}{6H_\eta E_D}\left(\frac{c}{r_p}\eta - sin\frac{c}{r_p}\eta\right) + \tau_p \tag{19}$$

According to the law of energy conservation, the covariance divergence of the stress-energy tensor vanishes, $\Delta_v T^{uv}$, thus, $\frac{\dot{a}}{a} T_u^u + 3\frac{\dot{a}}{a}\rho - i\frac{\partial\rho}{\partial\tau} = 0$, $3\left(\rho + \frac{P}{c^2}\right)\frac{\dot{a}}{a} - i\frac{\partial\rho}{\partial\tau} = 0$. By combining these outcomes, integrating, and substituting the spatial scale factor rate in Equation (17) to their outcome, the matter density evolution is

$$\rho\,(\eta) = D_p\left(1 - cos\frac{c}{r_p}\eta\right)^{-3} \tag{20}$$

where D_p is a constant.

Preprints (www.preprints.org) | NOT PEER-REVIEWED | Posted: 29 December 2022 doi:10.20944/preprints202005.0250.v11

According to Equation (14), the acceleration/deceleration of the Universe expansion, $\ddot{a}$, relies on the evolution in both the Universe's density and its scale factor. By rewriting Equation (14) in terms of the Hubble parameter rate, $\dot{H}$, by its definition at τ_p as

$$\int_{H_P}^{H} \dot{H}_\eta = \int_0^\eta -\frac{4\pi G_p D_p}{3a_p}\left(1 - cos\frac{c}{r_p}\eta\right)^{-3} d\eta \tag{21}$$

By integrating using the Weierstrass substitution, the Hubble parameter evolution is

$$H_{\eta,m} = H_m\left(\frac{1}{3}cot^3\frac{c}{2r_p}\eta + cot\frac{c}{2r_p}\eta\right) + H_p \tag{22}$$

where H_m and H_p are integration constants. The Hubble parameter evolution for radiation-only can be obtained by using Equations (14) and the procedure of Equation (20):

$$H_{\eta,r} = H_r\left(\frac{1}{5}cot^5\frac{c}{2r_p}\eta + \frac{2}{3}cot^3\frac{c}{2r_p}\eta + cot\frac{c}{2r_p}\eta\right) + H_p \tag{23}$$

where H_r is a constant. The quantized field equations in Equation (8) can be interpreted as conceptualizing that a 4D conformal bulk, as a manifestation of vacuum energy, embeds a 4D relativistic cloud-world representing a celestial object of a conventional time flow that in turns encapsulates 4D relativistic quantum clouds and so forth. As quantum time is quantized in the conventional time, analogously, the latter should be quantized in the conformal time. The early Universe metric can be expressed in terms of conformal time as $ds^2 = a^2/{a_p}^2\left(c^2d\eta^2 - dr^2/(1 - r^2/{r_p}^2) - r^2\,d\theta^2 - r^2sin^2\theta\,d\phi^2\right)$. The wavefunction of the Universe could be obtained by utilizing the quantized field equations as

$$i\hbar\gamma^\mu\partial_\mu\psi - \frac{1}{2}i\hbar\gamma^\mu\partial^\nu\frac{a^2}{{a_p}^2}\left(c^2 - \left(1 - \frac{r^2}{{r_p}^2}\right)^{-1} - r^2 - r^2sin^2\theta\right)\psi - (J^\mu A_\mu - \frac{1}{2}J^\mu A^\nu\zeta_{\mu\nu})\psi = \frac{1}{2}\frac{\hbar}{x^\mu}R\partial_R\psi \tag{24}$$

where $\eta = a_p t/a$ is the conformal time. Also, The wavefunction with respects to its reference value ψ_p can be obtained by using the scale factor and imaginary time evolution:

$$\frac{\psi(\eta)}{\psi_p} = \mp\frac{E_p}{6E_D}\left(\left(1 - cos\frac{c}{r_p}\eta\right)^2 + \frac{c^2}{{H_\eta}^2 a_p^2}\left(\frac{c}{r_p}\eta - sin\frac{c}{r_p}\eta\right)^2\right)^{1/2} exp\,cot^{-1}|H_\eta|\frac{a_p - a_p\,cos\,c\eta/r_p}{c^2\eta/r_p - c\,sin\,c\eta/r_p} \tag{25}$$

where $E/6E_D$ in denotes a new dimensionless energy parameter as the ratio of the early Universe energy density E_p to the vacuum energy density E_D.

4. Evolution of the Universe

The positive and negative solutions of the wavefunction ψ_L imply that matter and antimatter of the plasma evolved in opposite directions. The evolution of the Universe according to the wavefunction for both matter and radiation-only in addition to the light cone are shown in Figure 2a; where only the positive solution of one Universe side is shown due to their symmetry. A chosen mean evolution value of the Hubble parameter of ~70 km·s-1·Mpc-1 and a phase transition of expansion at an age of ~10 Gyr were applied to tune the integration constants of the model; the predicted energy density parameter is ~1.16. Further, the Hubble parameter evolution and its rate shown in Figure 2b.

Preprints (www.preprints.org) | NOT PEER-REVIEWED | Posted: 29 December 2022 doi:10.20944/preprints202005.0250.v11

According to the wavefunction (Figure 2a, orange curve), the cosmic evolution can be interpreted as comprising three distinct phases. Firstly, matter and antimatter sides expand in opposite directions away from early plasma during the first phase perhaps due to the phenomenon of plasma drift in the presence of electromagnetic fields. The expansion speed shown in Figure 2b (blue curve) starts with a hyperbolic rate at the nascent stages, then, the rate decreases due to gravity between the two sides, until it reached its minimal at the phase transition at an age of ~ 10 Gyr.

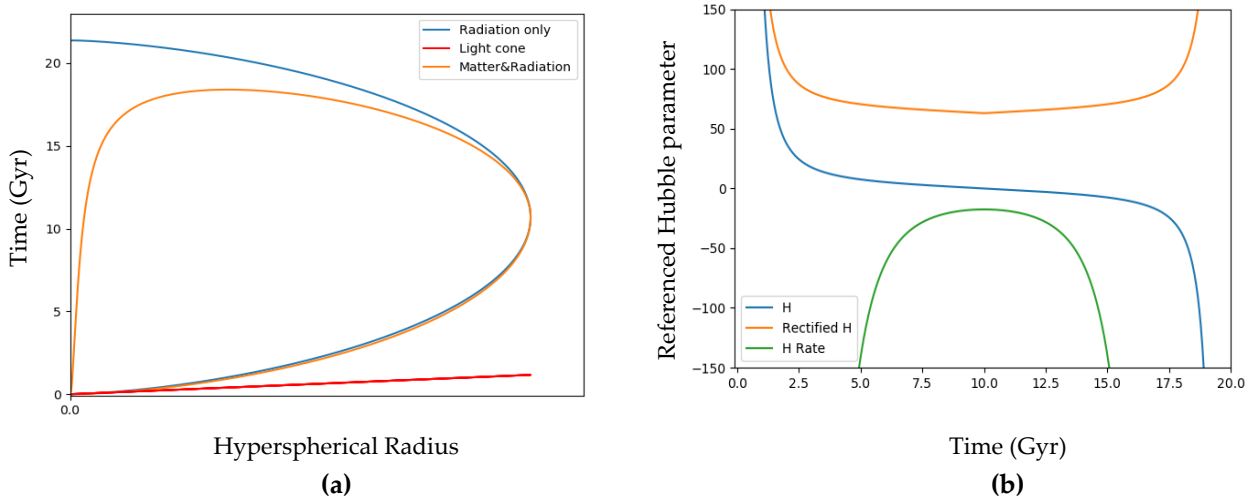

Figure 2. (**a**) Evolution of the wavefunction of matter of one side of the Universe, radiation only wavefunction, in addition to the straight line of light cone (diagram is not to scale). (**b**) The Hubble parameter H evolution and its rate.

However, the matter wavefunction reverses its direction in the second phase with both sides of matter and antimatter entering a state of free-fall towards each other at gravitational acceleration possibly causing current accelerated expansion; the Hubble parameter starts to increase in this phase.

Figure 3a shows a visualization of the wavefunction possibility explaining the dark flow while the apparent Universe geometry due to the gravitational lensing effects in Figure 3b is possibility matching the SLOAN Digital Sky Survey data virtualization [23].

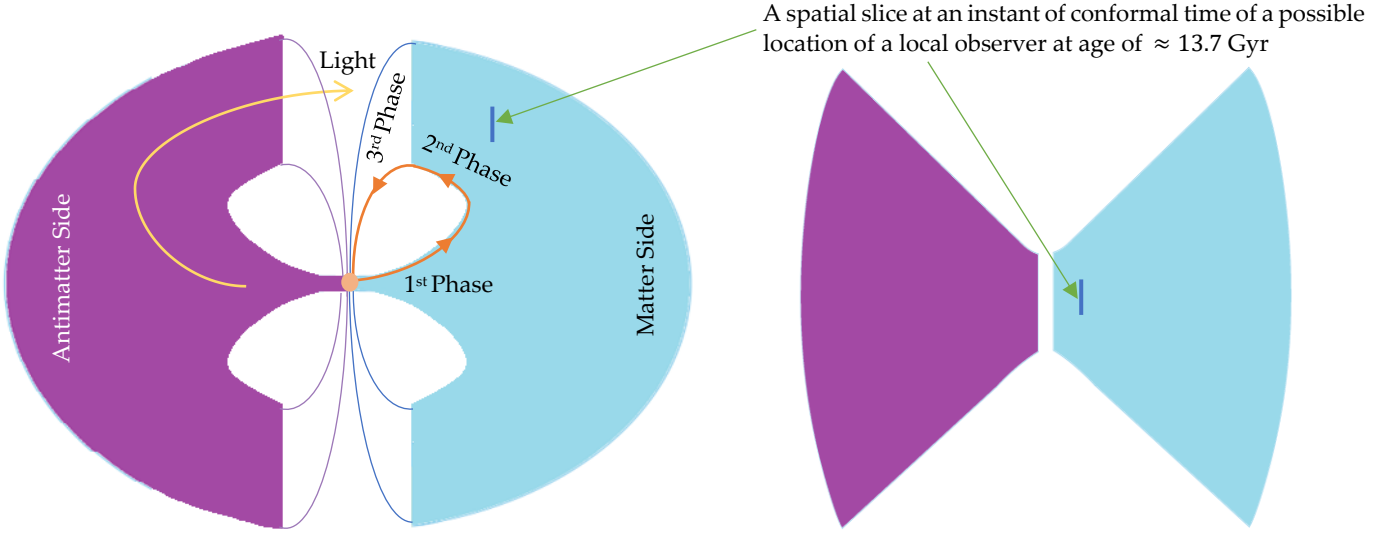

Figure 3. (**a**) A schematic 2D spatial and 1D temporal dimensions of the predicted cosmic topology of both sides where the expansion at the first phase is away from the early plasma while the second phase is corresponding to the reversal of the expansion direction. The future third phase corresponds to a spatial contraction leading to a Big Crunch. (**b**) The apparent topology during the first and second phases caused by the gravitational lensing effects.

Preprints (www.preprints.org) | NOT PEER-REVIEWED | Posted: 29 December 2022 doi:10.20944/preprints202005.0250.v11

According to mechanics, the minus sign of the expansion speed in the second phase (Figure 2b, blue curve) indicates an opposite direction. In addition, the opposite signs of the acceleration (Figure 2b, green curve) and the speed in the first phase indicate a slowing down while the matching signs in the second phase indicate the speed of expansion is increasing. Interestingly, the matter wavefunction predicts a final phase of spatial contraction that appears after ~18 Gyr, which could be because of the future high concentration of matter/antimatter at both sides that culminates in a Big Crunch, signaling a cyclic Universe. On the other hand, the radiation-only according to its wave function, which propagates faster than matter, is predicted to pass from a side to another side (See Figure 2a, blue curve), which could explain why the CMB can be observed even though matter moves much slower than light.

Regarding the present space-time flatness, the simulation of the congruence of space-time worldlines coupled with an initial flat or positive curvature has produced a curved geometry in the first phase, which is in agreement with the PL18 release [1,3] where the ends of the worldlines are not equal at any age during the first phase shown in Figure 4a. Conversely, at the accelerated expansion phase in the reverse directions, the simulation of the worldlines coupled with initial positive curvature produced equal worldlines or a flat spacetime as shown in Figure 4b.

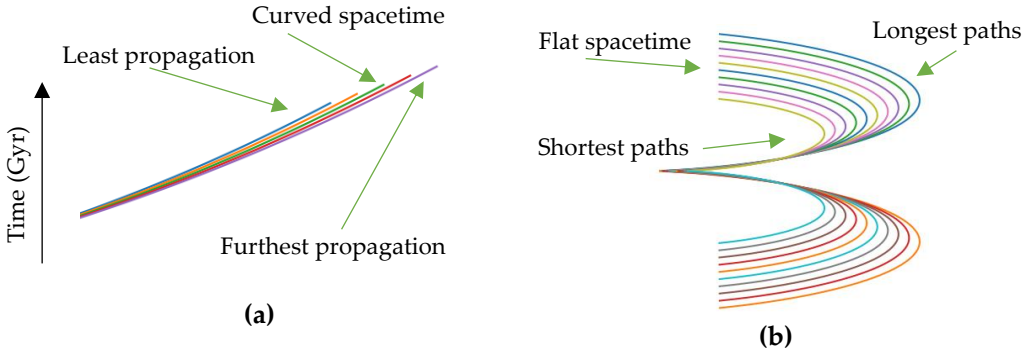

Figure 4. Evolution of spacetime worldlines at (**a**) early and **(b)** present Universe.

This is because that the worldlines that propagate the furthest due to initial curvature at the first phase, take longest paths at the second phase due to the reverse directions and vice versa. Further, Figure 5 shows 3D spatial and 1D temporal view of the dual Universe.

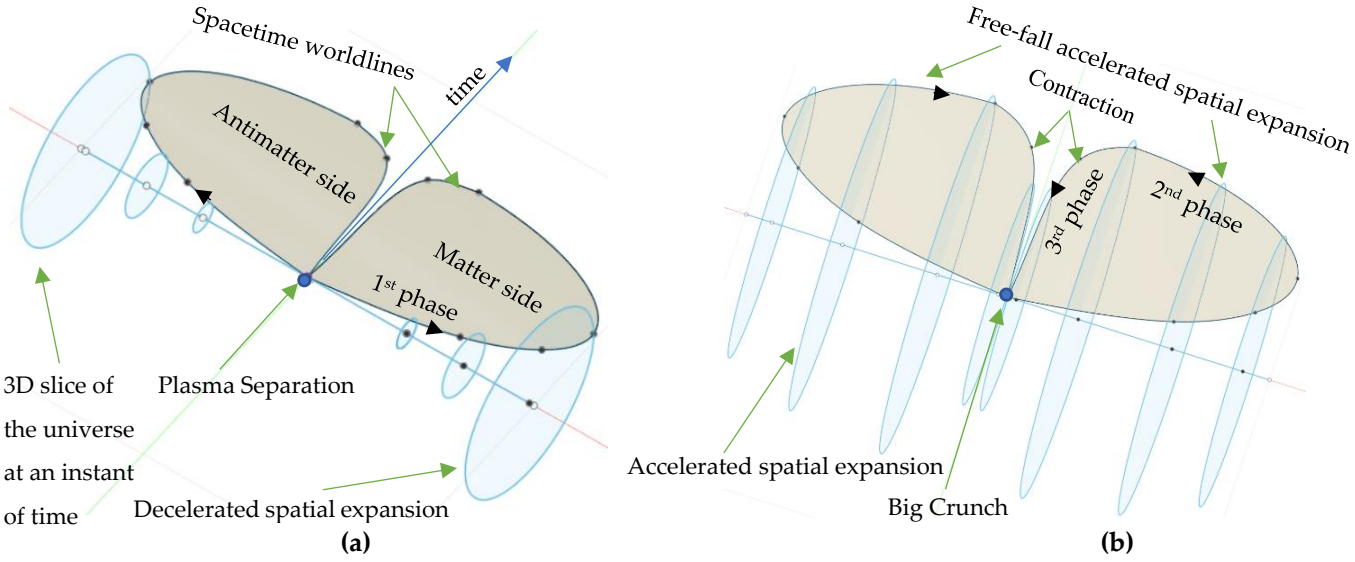

Figure 5. A schematic in 3D spatial and 1D temporal dimensions of both Universe sides. **(a)** 1st **(b)** 2nd and 3rd phases.

Preprints (www.preprints.org) | NOT PEER-REVIEWED | Posted: 29 December 2022 doi:10.20944/preprints202005.0250.v11

5. Galaxy Formation, Evolution, and Rotation under External Fields

Observations from the Deep Extragalactic Evolutionary Probe 2 Survey of a large sample of disk galaxies found that the motion of galaxies was steadily getting in order with their rotation velocity increasing over the last eight billion years [24,25]. In addition, galactic rotation curves were found to be influenced by external fields [26] and follow the baryonic Tully-Fisher relation [27,28]. On the other hand, several studies reported that some galaxies are missing dark matter [29–31]. To get insights from these observations while aiming to present a new galaxy formation scenario considering the background curvature as preferred by the PL18 release by utilizing the extended field equations as 4D relativistic Cloud-World that flows and spins through the 4D conformal bulk of a curvature evolving over the conformal time. The wavefunction showed the early Universe expanded hyperbolically at nascent stages.

The entire contribution comes from the boundary term when calculating the black hole entropy using the semiclassical approach [10,11]. Applying this concept and by rearranging the field equations for this setting as

$$R_{\mu\nu} - \frac{1}{2}Rg_{\mu\nu} - \frac{R\mathcal{R}_{\mu\nu}}{\mathcal{R}} = \frac{8\pi G_{\mathcal{R}}}{c^4}\hat{T}_{\mu\nu} - \frac{R(\mathcal{K}_{\mu\nu} - \frac{1}{2}\mathcal{K}\hat{q}_{\mu\nu}) - \mathcal{R}(K_{\mu\nu} - \frac{1}{2}K\hat{q}_{\mu\nu})}{\mathcal{R}^2} = 0 \quad (26)$$

Equation (26) gives

$$R_{\mu\nu} = \frac{1}{2}Rg_{\mu\nu} + R\frac{\mathcal{R}_{\mu\nu}}{\mathcal{R}} = \frac{1}{2}R\left(g_{\mu\nu} + 2\tilde{g}_{\mu\nu}\right) = \frac{1}{2}Rg_{\mu\nu}(1 + 2\Omega^2) = 0 \quad (27)$$

where $\hat{g}_{\mu\nu} = g_{\mu\nu} + 2\tilde{g}_{\mu\nu}$ and $\tilde{g}_{\mu\nu} = \mathcal{R}_{\mu\nu}/\mathcal{R} = \mathcal{R}_{\mu\nu}/\mathcal{R}_{\mu\nu}\tilde{g}^{\mu\nu}$ is the conformal bulk metric, which can be expressed as proportional to cloud-world metric $g_{\mu\nu}$ as $\tilde{g}_{\mu\nu} = g_{\mu\nu}\Omega^2$ by utilizing Ω^2, the conformal transformation function. The conformally transformed metric $\hat{g}_{\mu\nu} = g_{\mu\nu}(1 + 2\Omega^2)$ can be expressed as

$$ds^2 = -A(r)\left(1 + 2\Omega^2(r,r)\right)c^2dt^2 + S^2\left(B(r)\left(1 + 2\Omega^2(r,r)\right)dr^2 + r^2d\theta^2 + r^2sin^2\theta\, d\phi^2\right) \quad (28)$$

where A, B, S and Ω^2 are functions of the radius r; S is a dimensionless conformal scale factor. The derived conformal metric in Appendix B is

$$ds^2 = \left(1 - \frac{r_s}{r} - \frac{r_p}{r}\right)\left(-c^2dt^2 + S^2\left(\frac{dr^2}{1 + \frac{r_s^2}{r^2} - 2\frac{r_s}{r}} + \frac{r^2d\theta^2 + r^2sin^2\theta d\phi^2}{1 - \frac{r_s}{r} - \frac{r_p}{r}}\right)\right) \quad (29)$$

This metric reduces to the Schwarzschild metric in a flat background ($r \to \infty$). In the case of PI18's preferred early Universe positive curvature, the gravitational potential of the bulk can be expressed in terms of the early Universe plasma of mass, M_p, and r denoting the radius of curvature of the bulk, where the bulk's potential decreases with the Universe expansion and vanishes in the flat spacetime background ($r \to \infty$). The minus sign of Ω^2 reveals a spatial shrinking through evolving in the conformal time, which agrees with the vortex model that can occur due to the high-speed spinning. The metric can be visualized by using Flamm's approach as

$$\mathcal{W}(r,r) = \mp\int \frac{\sqrt{\left(\frac{r_s}{r} - \frac{r_s^2}{r^2} - \frac{r_p}{r}\right)}}{\left(1 - \frac{r_s}{r}\right)}dr = \mp\sqrt{r_s(r - r_s) - r_p\frac{r^2}{r}} + \mathcal{O} + C \quad (30)$$

where C is a constant and $\mathcal{O}$ denotes less significant terms.

Preprints (www.preprints.org) | NOT PEER-REVIEWED | Posted: 29 December 2022 doi:10.20944/preprints202005.0250.v11

The visualization of Equation (30) of this scenario of the galaxy formation as a forced vortex due to the curvature of the background is shown in Figure 6, the evolution of the 4D cloud-world of metric $g_{\mu\nu}$ through its travel and spin in the conformal space-time of the 4D bulk of metric $\tilde{g}_{\mu\nu}$.

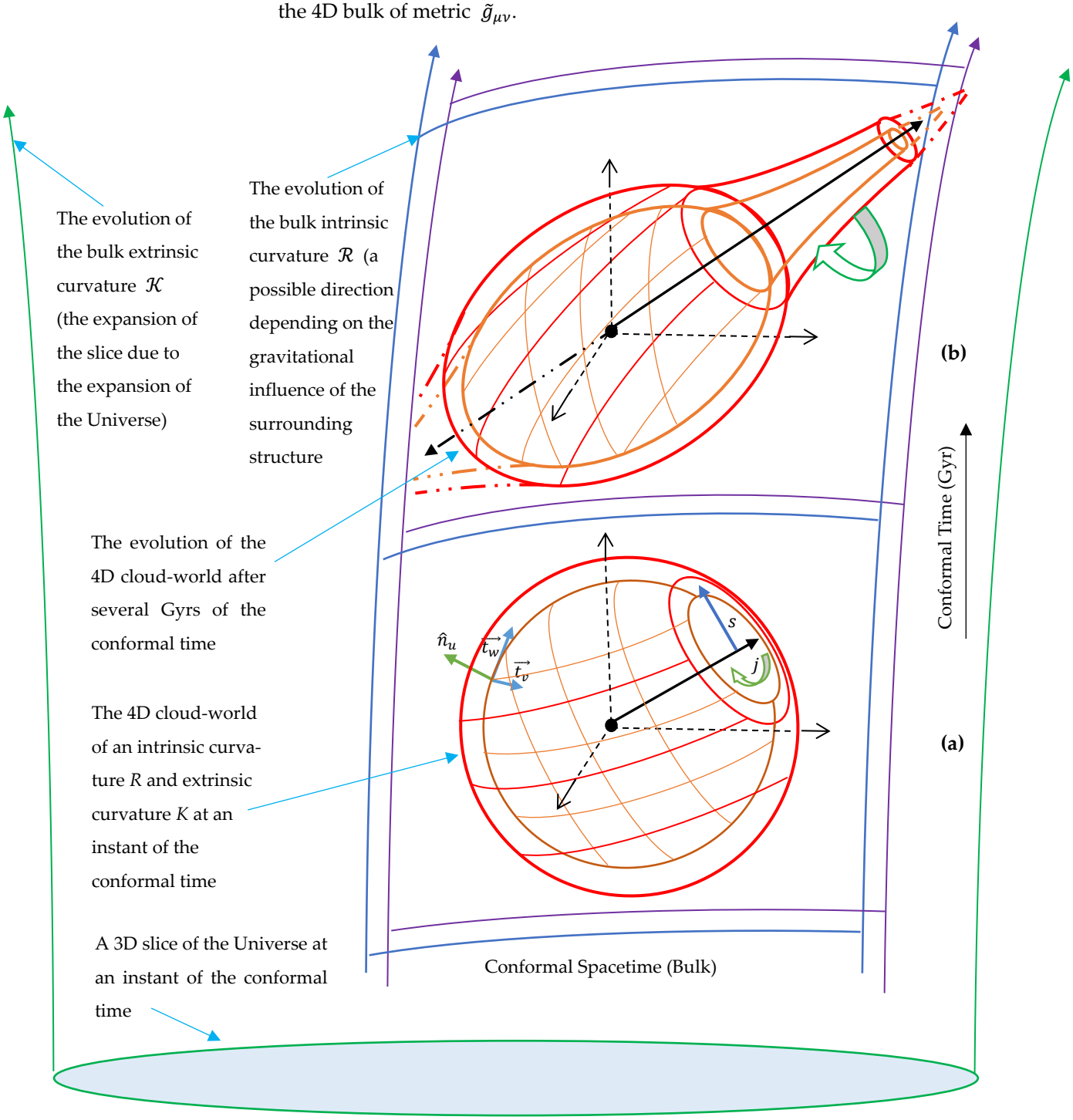

Figure 6. The hypersphere of a compact core of a galaxy (the red-orange 4D cloud-world) along with its travel and spin through the conformal spacetime (the blue-purple 4D bulk representing the bulk of distinctive curvature evolving over the conformal time.

Preprints (www.preprints.org) | NOT PEER-REVIEWED | Posted: 29 December 2022 doi:10.20944/preprints202005.0250.v11

This scenario of galaxy formation indicates that the core of the galaxy forms a central event horizon leading to opposite traversable wormholes spatially shrinking through the conformal time in the bulk. The galaxy and its core form at the same process while the gas clouds outside the core would form the spiral arms where the fast-rotating core induces frame dragging [34]. This could explain the formation of supermassive compact cores with a mass of ~10^9 $M_\odot$ at just 6% of the current Universe age [35]; thus, it could solve the black-hole hierarchy problem. Further, the observation of the superluminal motion in the x-ray jet of M87 [37] could be travel through these traversable wormholes (vortices). These findings are consistent with the observations of high-energy structures perpendicular to the central plane of the disk galaxies [38,39]. Additionally, orbiting a vortex can explain the orbit of the G2 cloud that just faced drag forces [41].

To evaluate the influence of the spinning momentum and the curvature of the background on the core of the galaxy and the surrounding gas clouds (the spiral arms), a fluid simulation was performed based on Newtonian dynamics by using the Fluid Pressure and Flow software [40]. In this simulation, the fluid was deemed to represent the space-time continuum throughout incrementally flattening curvature paths representing conformal curvature evolution to analyze the external momenta exerted on objects flowing throughout the incrementally flattening curvatures. The momenta yielded by the fluid simulation were used to simulate a spiral galaxy as a forced vortex (under external fields).

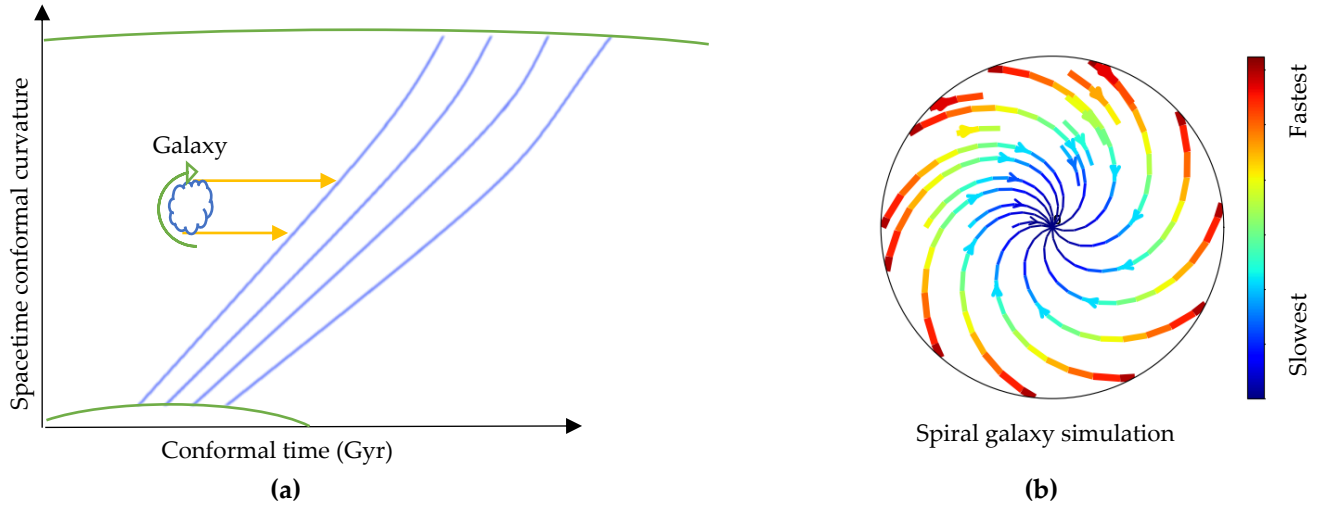

Figure 7. (**a**) External fields exerted on a galaxy due to the space-time conformal curvature evolution. Green curves represent the curvature of space-time worldlines. Blue curves represent the simulated space-time continuum flux. (**b**) Simulation of spiral galaxy rotation. Blue represents the slowest tangential speeds and red represents the fastest speeds.

The simulation shows that the tangential speeds of the outer parts of the spiral galaxy are rotating faster in comparison with the rotational speeds of the inner parts, which is consistent with observations of galaxy rotation. Since the rotation speed only depends on the galaxy mass and the background curvature, the findings are consistent with the baryonic Tully-Fisher relation and the detected external fields.

Preprints (www.preprints.org) | NOT PEER-REVIEWED | Posted: 29 December 2022 doi:10.20944/preprints202005.0250.v11

6. Early Universe Boundary Contribution

In the case of a closed early Universe, as preferred by PL18 [1,3,43], the gravitational contributions of the early Universe plasma boundary for high energy limits can be obtained by using the boundary term in the extended field equations. At the reference imaginary time τ_p, there is no conformal transformation. Therefore, the global $\mathcal{K}_{\mu\nu}$ and the local $K_{\mu\nu}$ boundaries are the same. Accordingly, the boundary term in the extended field equations reduces to

$$\frac{R-\mathcal{R}}{\mathcal{R}}\left(\mathcal{K}_{\mu\nu}-\frac{1}{2}\mathcal{K}\hat{q}_{\mu\nu}\right)=\frac{8\pi G_t}{c^4}T_{\mu\nu} \tag{31}$$

For smooth hypersphere of early plasma, the induced metric $\hat{q}_{\mu\nu}$ on its boundary is

$$[\hat{q}_{\mu\nu}]=diag\left(-c^2,\frac{a^2(t)}{{a_p}^2}R^2,\frac{a^2(t)}{{a_p}^2}R^2sin^2\theta\right), \tag{32}$$

where R is the extrinsic radius of curvature [32]. The extrinsic curvature tensor can be obtained by utilising the formula $\mathcal{K}_{uv}=-\overrightarrow{t_v}.\nabla_u\hat{n}_u$. Due to the smoothness of the hypersphere, the covariant derivative reduces to a partial derivative as $\mathcal{K}_{uv}=-\overrightarrow{t_v}\,\partial\hat{n}_u/\partial\overrightarrow{t^u}$ [32]. The extrinsic curvature tensor at τ_p is

$$[\mathcal{K}_{\mu\nu}]=diag\left(0,-\frac{a^2(t)}{{a_p}^2}R,-\frac{a^2(t)}{{a_p}^2}Rsin^2\theta\right) \tag{33}$$

The trace of the extrinsic curvature is $\mathcal{K}=\mathcal{K}_{\mu\nu}q^{\mu\nu}=2/R$. To convert the extrinsic curvature into intrinsic as follows $2/R\equiv 2/r_p^2$.

The bulk curvature of early Universe plasma boundary at τ_p is $\mathcal{R}_p=1/r_p^2$. On the other hand, the Ricci scalar curvature R_p at τ_p can be written in terms of the difference between kinetic and potential energy densities whereby substituting Friedmann equations in Equations (13) and (14) into the Ricci scalar curvature in Equation (12) as

$$R_p=\frac{6G_p}{c^2}\left(\frac{4\pi P_p}{c^2}-\frac{4\pi\rho_p}{3}\right) \tag{34}$$

By solving the boundary term for a perfect fluid given by $T_{\mu\nu}=(\rho+\frac{P}{c^2})\,u_\mu u_\nu+Pg_{\mu\nu}$ [19], and then substituting Equations (31) - (33) into the boundary term in Equation (31) as

$$\frac{\frac{6G_p}{c^2}\left(\frac{4\pi P_p}{c^2}-\frac{4\pi\rho_p}{3}\right)-\frac{1}{r_p^2}}{1/r_p^2}\left(\frac{-c^2}{r_p^2}\right)=8\pi G_p\rho_p \tag{35}$$

By multiplying both sides by early Universe plasma volume V_p, yields

$$r_p=\frac{4G_p\,P_pV_p}{c^4} \tag{36}$$

The reference radius of curvature $r_p>0$ because any reduction in the early plasma volume causes an increase in its pressure, which can realise a singularity-free paradigm. The smallest possible reference radius of the early Universe plasma due to its boundary gravitational contributions can reveal that the early Universe expansion upon emission of the CMB could mark the beginning of the Universe from a previously collapsed one. This in agreement with the wavefunction prediction of an eventual phase comprising rapid spatial contraction that culminates in a Big Crunch, signalling a cyclic Universe.

 doi:10.20944/preprints202005.0250.v11

7. Conclusions and Future Works

In this study, the background curvature is incorporated to extend the field equations where a closed early Universe model is considered by utilizing a referenced Friedmann–Lemaître metric model incorporating the scale factor of the early Universe and its radius of curvature upon the emission of the CMB. The evolution of the Universe from early plasma is modelled by utilizing a new wavefunction of the Universe. The wavefunction revealed both positive and negative solutions. This characteristic implies that a pair of entangled wavefunctions was created and evolved in opposite directions as a manifestation of distinct matter and antimatter sides of the Universe.

The wavefunction indicates a nascent hyperbolic expansion away from early energy is followed by a first phase of decelerating expansion during the first ~10 Gyr, and then, a second phase of accelerating expansion in reverse directions, whereby both sides free-fall towards each other under gravitational acceleration. This can explain the effects attributed to dark energy and the observed dark flow wheras dark energy was found either not constant or the Universe is expanding faster than estimated by the standard model. Additionally, the wavefunction predicted an eventual phase of rapid spatial contraction that culminates in a Big Crunch, signaling a cyclic Universe.

The predicted background curvature evolution demonstrated the fast orbital speed of outer stars owing to external fields exerted on galaxies as they travelled through earlier conformally curved spacetime. This can explain the effects attributed to dark matter. The evolution of $G_{\mathcal{R}}$ could explain the galaxy formation without involving dark matter where it was larger during the first phase of expansion.

The simulated spacetime worldlines during the decelerating phase were found to be flattened during the accelerating phase due to the reverse direction of the continuum worldlines. This can explain the current spacetime flatness. The radiation only worldlines predicted to pass from one side to another, which can explain why CMB radiation can be observed even though matter moves much slower than light while the apparent cosmic topology is possibly in accordance the SLOAN Digital Sky Survey data.

The wavefunction predicted a final phase of spatial contraction leading to a Big Crunch, signalling a cyclic Universe while the derived smallest possible radius of the early Universe plasma due to its boundary gravitational contributions can reveal that the early Universe expansion upon emission of the CMB could mark the beginning of the Universe from a previous collapse one. These findings reveal that early plasma could be separated and evolved into distinct sides of the Universe that collectively and geometrically inducing its evolution, physically explaining the effects attributed to dark matter and energy. Finally, this theoretical work will be tested against observational data in future works.

Acknowledgements: I am grateful to the MDPI/Preprints Editors Ms Mila Marinkovic and Ms Bojana Djokic for their rapid and excellent processing of a series of preprints during this work development.

Conflicts of Interest: The author declares no conflict of interest.

 doi:10.20944/preprints202005.0250.v11

Appendix A

The referenced metric and its inverse are

$$g_{\mu\nu} = \begin{pmatrix} c^2 & 0 & 0 & 0 \\ 0 & -\frac{\left(\frac{a^2}{a_p{}^2}\right)}{\left(1-\frac{r^2}{r_p{}^2}\right)} & 0 & 0 \\ 0 & 0 & -\left(\frac{a^2}{a_p{}^2}\right)r^2 & 0 \\ 0 & 0 & 0 & -\left(\frac{a^2}{a_p{}^2}\right)r^2 sin^2\theta \end{pmatrix} \tag{A.1}$$

$$g^{uv} = \begin{pmatrix} \frac{1}{c^2} & 0 & 0 & 0 \\ 0 & -\frac{\left(1-\frac{r^2}{r_p{}^2}\right)}{\left(\frac{a^2}{a_p{}^2}\right)} & 0 & 0 \\ 0 & 0 & \frac{-1}{\left(\frac{a^2}{a_p{}^2}\right)r^2} & 0 \\ 0 & 0 & 0 & \frac{-1}{\left(\frac{a^2}{a_p{}^2}\right)r^2 sin^2\theta} \end{pmatrix} \tag{A.2}$$

The Ricci curvature tensor R_{uv} is solved using the Christoffel symbols of the second kind which is given by $\Gamma^{\rho}_{\mu\nu} = \frac{1}{2}g^{\rho\lambda}(\partial_\mu g_{\lambda\nu} + \partial_\nu g_{\lambda\mu} - \partial_\lambda g_{\mu\nu})$ for the referenced metric tensor $g_{\mu\nu}$. The non-zero Christoffel symbols are:

$$\Gamma^0{}_{11} = \frac{a\dot{a}}{c^2 a_p{}^2\left(1-\frac{r^2}{r_p{}^2}\right)} \tag{A.3}$$

$$\Gamma^0{}_{22} = \frac{r^2 a\dot{a}}{c^2 a_p{}^2} \tag{A.4}$$

$$\Gamma^0{}_{33} = \frac{r^2 a\dot{a}\, sin^2\theta}{c^2 a_p{}^2} \tag{A.5}$$

$$\Gamma^1{}_{11} = \frac{\mathrm{r}}{r_p{}^2\left(1-\frac{r^2}{r_p{}^2}\right)} \tag{A.6}$$

$$\Gamma^1{}_{22} = -\mathrm{r}\left(1-\frac{r^2}{r_p{}^2}\right) \tag{A.7}$$

Preprints (www.preprints.org) | NOT PEER-REVIEWED | Posted: 29 December 2022 doi:10.20944/preprints202005.0250.v11

$$\Gamma^1{}_{33} = -\mathrm{r}sin^2\theta\left(1-\frac{r^2}{r_p{}^2}\right) \tag{A.8}$$

$$\Gamma^1{}_{01} = \Gamma^2{}_{02} = \Gamma^3{}_{03} = \Gamma^1{}_{10} = \Gamma^2{}_{20} = \Gamma^3{}_{30} = \frac{\dot{a}}{a} \tag{A.9}$$

$$\Gamma^2{}_{12} = \Gamma^2{}_{21} = \Gamma^3{}_{13} = \Gamma^3{}_{31} = \frac{1}{r} \tag{A.10}$$

$$\Gamma^2{}_{33} = -sin\,\theta\,cos\theta \tag{A.11}$$

$$\Gamma^3{}_{23} = \Gamma^3{}_{32} = cot\,\theta \tag{A.12}$$

The Ricci curvature tensor given by $R_{\mu\nu} = \partial_\lambda\Gamma^\lambda{}_{\mu\nu} - \partial_\nu\Gamma^\lambda{}_{\mu\lambda} + \Gamma^\rho{}_{\mu\nu}\Gamma^\lambda{}_{\rho\lambda} - \Gamma^\rho{}_{\mu\lambda}\Gamma^\lambda{}_{\rho\nu}$. The non-zero components are solved as follows.

The $t-t$ component is

$$R_{tt} = R_{00} = -\partial_0\Gamma^1{}_{01} - \partial_0\Gamma^2{}_{02} - \partial_0\Gamma^3{}_{03} - \Gamma^1{}_{01}\Gamma^1{}_{10} - \Gamma^2{}_{02}\Gamma^2{}_{20} - \Gamma^3{}_{03}\Gamma^3{}_{30} \tag{A.13}$$

$$R_{tt} = -3\partial_t\frac{\dot{a}}{a} - 3\left(\frac{\dot{a}}{a}\right)^2 = -3\frac{\ddot{a}a - \dot{a}^2}{a^2} - 3\frac{\dot{a}^2}{a^2} = -3\frac{\ddot{a}}{a} \tag{A.14}$$

The $r-r$ component of the Ricci tensor is

$$\begin{aligned} R_{rr} = R_{11} = {} & \partial_0\Gamma^0{}_{11} - \partial_1\Gamma^2{}_{12} - \partial_1\Gamma^3{}_{13} + \Gamma^0{}_{11}\Gamma^2{}_{02} + \Gamma^0{}_{11}\Gamma^3{}_{03} - \Gamma^1{}_{10}\Gamma^0{}_{11} \\ & + \Gamma^1{}_{11}\Gamma^2{}_{12} + \Gamma^1{}_{11}\Gamma^3{}_{13} \end{aligned} \tag{A.15}$$

$$R_{rr} = \partial_t\frac{a\dot{a}}{c^2a_p{}^2\left(1-\frac{r^2}{r_p{}^2}\right)} - 2\partial_r\frac{1}{r} + \frac{a\dot{a}}{c^2a_p{}^2\left(1-\frac{r^2}{r_p{}^2}\right)}\frac{\dot{a}}{a} + 2\frac{\mathrm{r}}{r_p{}^2\left(1-\frac{r^2}{r_p{}^2}\right)}\frac{1}{r} - 2\frac{1}{r^2} \tag{A.16}$$

$$R_{rr} = \frac{a\ddot{a}}{c^2a_p{}^2\left(1-\frac{r^2}{r_p{}^2}\right)} + \frac{\dot{a}^2}{c^2a_p{}^2\left(1-\frac{r^2}{r_p{}^2}\right)} + \frac{\dot{a}^2}{c^2a_p{}^2\left(1-\frac{r^2}{r_p{}^2}\right)} + \frac{2}{r_p{}^2\left(1-\frac{r^2}{r_p{}^2}\right)} \tag{A.17}$$

$$R_{rr} = \frac{\left(\frac{a\ddot{a}}{a_p{}^2} + \frac{2\dot{a}^2}{a_p{}^2} + \frac{2c^2}{r_p{}^2}\right)}{c^2\left(1-\frac{r^2}{r_p{}^2}\right)} \tag{A.18}$$

The $\theta-\theta$ component is

$$\begin{aligned} R_{\theta\theta} = R_{22} = {} & \partial_0\Gamma^0{}_{22} + \partial_1\Gamma^1{}_{22} - \partial_2\Gamma^3{}_{23} + \Gamma^0{}_{22}\Gamma^1{}_{01} + \Gamma^0{}_{22}\Gamma^3{}_{03} + \Gamma^1{}_{22}\Gamma^1{}_{11} \\ & + \Gamma^1{}_{22}\Gamma^3{}_{13} - \Gamma^2{}_{20}\Gamma^0{}_{22} - \Gamma^2{}_{21}\Gamma^1{}_{22} - \Gamma^3{}_{23}\Gamma^3{}_{32} \end{aligned} \tag{A.19}$$

Preprints (www.preprints.org) | NOT PEER-REVIEWED | Posted: 29 December 2022 doi:10.20944/preprints202005.0250.v11

$$R_{\theta\theta} = \partial_t \frac{r^2 a\dot{a}}{c^2 {a_p}^2} - \partial_r \mathrm{r}\left(1 - \frac{r^2}{{r_p}^2}\right) - \partial_\theta \cot(\theta) + \frac{r^2 a\dot{a}}{c^2 {a_p}^2}\frac{\dot{a}}{a} - \mathrm{r}\left(1 - \frac{r^2}{{r_p}^2}\right)\frac{1}{r} - \cot^2(\theta) \tag{A.20}$$

$$R_{\theta\theta} = \frac{r^2 a\ddot{a}}{c^2 {a_p}^2} + \frac{r^2 \dot{a}^2}{c^2 {a_p}^2} + \left(3\frac{r^2}{{r_p}^2} - 1\right) + \csc^2(\theta) + \frac{r^2 \dot{a}^2}{c^2 {a_p}^2} - \left(1 - \frac{r^2}{{r_p}^2}\right) - \cot^2(\theta) \tag{A.21}$$

$$R_{\theta\theta} = \frac{r^2 a\ddot{a}}{c^2 {a_p}^2} + 2\frac{r^2 \dot{a}^2}{c^2 {a_p}^2} + \left(2\frac{r^2}{{r_p}^2}\right) - 1 + \csc^2(\theta) - \cot^2(\theta) \tag{A.22}$$

$$R_{\theta\theta} = \frac{r^2}{c^2}\left(\frac{a\ddot{a}}{{a_p}^2} + \frac{2\dot{a}^2}{{a_p}^2} + \frac{2c^2}{{r_p}^2}\right) \tag{A.23}$$

The $\phi - \phi$ component is

$$R_{\phi\phi} = R_{33} = \partial_0 {\Gamma^0}_{33} + \partial_1 {\Gamma^1}_{33} + \partial_2 {\Gamma^2}_{33} + {\Gamma^0}_{33}{\Gamma^1}_{01} + {\Gamma^0}_{33}{\Gamma^2}_{02} + {\Gamma^1}_{33}{\Gamma^1}_{11} + {\Gamma^1}_{33}{\Gamma^2}_{12} - {\Gamma^3}_{30}{\Gamma^0}_{33} - {\Gamma^3}_{31}{\Gamma^1}_{33} - {\Gamma^3}_{32}{\Gamma^2}_{33} \tag{A.24}$$

$$R_{\phi\phi} = \partial_t \frac{r^2 a\dot{a}\sin^2\theta}{c^2 {a_p}^2} - \partial_r \mathrm{r}\sin^2\theta\left(1 - \frac{r^2}{{r_p}^2}\right) - \partial_\theta \sin\theta\cos\theta + 2\frac{r^2 a\dot{a}\sin^2\theta}{c^2 {a_p}^2}\frac{\dot{a}}{a} - \mathrm{r}\sin^2\theta\left(1 - \frac{r^2}{{r_p}^2}\right)\frac{\mathrm{r}}{{r_p}^2\left(1 - \frac{r^2}{{r_p}^2}\right)} - \mathrm{r}\sin^2\theta\left(1 - \frac{r^2}{{r_p}^2}\right)\frac{1}{r} - \frac{\dot{a}}{a}\frac{r^2 a\dot{a}\sin^2\theta}{c^2 {a_p}^2} + \mathrm{r}\sin^2\theta\left(1 - \frac{r^2}{{r_p}^2}\right)\frac{1}{r} + \sin\theta\cos\theta\cot\theta \tag{A.25}$$

$$R_{\phi\phi} = R_{33} = \frac{r^2 a\ddot{a}\sin^2\theta}{c^2 {a_p}^2} + \frac{r^2 \dot{a}^2 \sin^2\theta}{c^2 {a_p}^2} - \sin^2\theta\left(1 + 3\frac{r^2}{{r_p}^2}\right) + \sin^2\theta - \cos^2\theta + \frac{r^2 \dot{a}^2 \sin^2\theta}{c^2 {a_p}^2} - \sin^2\theta\left(\frac{r^2}{{r_p}^2}\right) + \cos^2\theta \tag{A.26}$$

$$R_{\phi\phi} = R_{33} = \frac{r^2 a\ddot{a}\sin^2\theta}{c^2 {a_p}^2} + 2\frac{r^2 \dot{a}^2 \sin^2\theta}{c^2 {a_p}^2} + 2\sin^2\theta\frac{r^2}{{r_p}^2} \tag{A.27}$$

$$R_{\phi\phi} = \frac{r^2 \sin^2\theta}{c^2}\left(\frac{a\ddot{a}}{{a_p}^2} + \frac{2\dot{a}^2}{{a_p}^2} + \frac{2c^2}{{r_p}^2}\right) \tag{A.28}$$

The Ricci scalar curvature is

$$R = R_{\mu\nu}\, g^{\mu\nu} = -\frac{6}{c^2}\left(\frac{\ddot{a}}{a} + \frac{\dot{a}^2}{a^2} + \frac{c^2\, {a_p}^2}{a^2\, {r_p}^2}\right) \tag{A.29}$$

where the dotes are time derivatives.

Preprints (www.preprints.org) | NOT PEER-REVIEWED | Posted: 29 December 2022 doi:10.20944/preprints202005.0250.v11

Appendix B

The conformally transformed metric $\hat{g}_{\mu\nu} = g_{\mu\nu}(1 + 2\Omega^2)$ can be expressed as

$$ds^2 = -A(r)\left(1 + 2\Omega^2(r,\mathcal{r})\right)c^2dt^2 + S^2\left(B(r)\left(1 + 2\Omega^2(r,\mathcal{r})\right)dr^2 + r^2d\theta^2 + r^2sin^2\theta\, d\phi^2\right) \quad \text{(B.1)}$$

where A and B are functions of the cloud-world radius r, S^2 is a dimensionless conformal scale factor. By performing the coordinate transformation as follows

$$ds^2 = -\left(A(\lambda) + 2A(\lambda)\Omega^2(\lambda,\mathcal{r})\right)c^2dt^2 + \left(B(\lambda) + 2B(\lambda)\Omega^2(\lambda,\mathcal{r})\right)d\lambda^2 + \lambda^2d\theta^2 + \lambda^2sin^2\theta\, d\phi^2 \quad \text{(B.1)}$$

where the conformal function Ω^2 is a function of the bulk radius of curvature $\mathcal{r}$ and it can be influenced by the cloud-world radius. The Christoffel symbols of this metric are

$$\Gamma^1_{00} = \frac{\dot{A}(1 + 2\Omega^2) + 4A\dot{\Omega}}{2(B + 2B\Omega^2)}, \qquad \Gamma^0_{01} = \frac{\dot{A}(1 + 2\Omega^2) + 4A\dot{\Omega}}{2(A + 2A\Omega^2)}, \quad \Gamma^1_{11} = \frac{\dot{B}(1 + 2\Omega^2) + 4B\dot{\Omega}}{2(B + 2B\Omega^2)}$$

$$\Gamma^1_{22} = \frac{-\lambda}{(B + 2B\Omega^2)}, \quad \Gamma^1_{33} = \frac{-\lambda sin^2\theta}{(B + 2B\Omega^2)}, \qquad \Gamma^2_{21} = \Gamma^2_{12} = \frac{1}{\lambda} \quad \text{(B.2)}$$

$$\Gamma^2_{33} = -\,sin\theta\, cos\theta, \quad \Gamma^3_{32} = \Gamma^3_{23} = \frac{cos\theta}{sin\theta}$$

where the sign $\dot{}$ is a total derivative of the function. The Ricci tensor components are

$$R_{tt} = -\frac{\ddot{A}\left(1 + 2\Omega^2 + 4\dot{\Omega}\right) + 4A\ddot{\Omega} + 4\dot{\Omega}\dot{A}}{2\left(B + 2B\Omega^2\right)} + \frac{\left(\dot{A}\left(1 + 2\Omega^2\right) + 4A\dot{\Omega}\right)\left(\dot{B}\left(1 + 2\Omega^2\right) + 4B\dot{\Omega}\right)}{4\left(B + 2B\Omega^2\right)^2} \quad \text{(B.3)}$$

$$+ \frac{\left(\dot{A}\left(1 + 2\Omega^2\right) + 4A\dot{\Omega}\right)^2}{4\left(A + 2A\Omega^2\right)\left(B + 2B\Omega^2\right)} - \frac{1}{\lambda}\frac{\dot{A}\left(1 + 2\Omega^2\right) + 4A\dot{\Omega}}{\left(B + 2B\Omega^2\right)}$$

$$R_{rr} = \frac{1}{2}\left(\frac{\ddot{A}\left(1 + 2\Omega^2 + 4\dot{\Omega}\right) + 4A\ddot{\Omega} + 4\dot{\Omega}\dot{A}}{\left(A + 2A\Omega^2\right)} - \frac{\left(\dot{A}\left(1 + 2\Omega^2\right) + 4A\dot{\Omega}\right)^2}{2\left(A + 2A\Omega^2\right)^2}\right) \quad \text{(B.4)}$$

$$- \frac{\left(\dot{A}\left(1 + 2\Omega^2\right) + 4A\dot{\Omega}\right)\left(\dot{B}\left(1 + 2\Omega^2\right) + 4B\dot{\Omega}\right)}{4\left(A + 2A\Omega^2\right)\left(B + 2B\Omega^2\right)} - \frac{1}{\lambda}\frac{\dot{B}\left(1 + 2\Omega^2\right) + 4B\dot{\Omega}}{B + 2B\Omega^2}$$

$$R_{\theta\theta} = \frac{1}{\left(B + 2B\Omega^2\right)} - \frac{\lambda}{2\left(B + 2B\Omega^2\right)}\left(\frac{\dot{B}\left(1 + 2\Omega^2\right) + 4B\dot{\Omega}}{\left(B + 2B\Omega^2\right)} - \frac{\dot{A}\left(1 + 2\Omega^2\right) + 4A\dot{\Omega}}{\left(A + 2A\Omega^2\right)}\right) - 1 \quad \text{(B.5)}$$

$$R_{\phi\phi} = \frac{sin^2\theta}{\left(B + 2B\Omega^2\right)} - \frac{\lambda sin^2\theta}{2\left(B + 2B\Omega^2\right)}\left(\frac{\dot{B}\left(1 + 2\Omega^2\right) + 4B\dot{\Omega}}{\left(B + 2B\Omega^2\right)} - \frac{\dot{A}\left(1 + 2\Omega^2\right) + 4A\dot{\Omega}}{\left(A + 2A\Omega^2\right)}\right) - sin^2\theta \quad \text{(B.6)}$$

Preprints (www.preprints.org) | NOT PEER-REVIEWED | Posted: 29 December 2022 doi:10.20944/preprints202005.0250.v11

By substituting Ricci tensor components in Equation (7) gives

$$\left(\dot{A}(1+2\Omega^2)+4A\dot{\Omega}\right)(B+2B\Omega^2)+(A+2A\Omega^2)\left(\dot{B}(1+2\Omega^2)+4B\dot{\Omega}\right)=0 \tag{B.8}$$

Equation (16) yields

$$B+2B\Omega^2=\frac{k}{A+2A\Omega^2} \tag{B.9}$$

where $k=1+4\Omega^2+\Omega^4$ for the conformal metric by considering the bulk curvature. By applying the weak-field limit: $\hat{g}_{\mu\nu}\approx\eta_{\mu\nu}+\hat{h}_{\mu\nu}$, as follows

$$\Gamma^i_{tt}=\frac{1}{2}\int\partial_i\hat{h}_{tt}=\frac{1}{c^2}\int\partial_i\varphi \tag{B.10}$$

where φ is the Newtonian gravitational potential. By integrating both sides

$$\hat{g}_{tt}=-A(1+2\Omega^2)=-\left(\eta_{tt}+\frac{2\varphi_c}{c^2}+\frac{2\varphi_b}{c^2}\right) \tag{B.11}$$

where $\varphi_c=-GM/\lambda$ is the gravitational potential of the cloud-world's spherical mass and φ_b that arises from the integration can be interpreted as the gravitational potential resulting from the bulk curvature, which can be expressed, using the same Newtonian analogue, in terms of the mass of the early Universe plasma of preferred positive curvature, M_p, and the bulk curvature radius $\mathfrak{r}$ as $\varphi_b=-G_pM_p/\mathfrak{r}$. The metric should yield only the gravitational potential of the cloud-world when there is no bulk curvature $(\Omega^2=0)$ and $(\varphi_b=0)$; hence, $A=(1+2\varphi_c/c^2)$; consequently, the conformal function is $\Omega^2=\varphi_b/Ac^2$. By performing the coordinate retransformation and combining Equations (17 - 19) yield

$$\Omega^2=-\frac{G_pM_p}{\mathfrak{r}c^2}\left(1-\frac{2GM}{rc^2}\right)^{-1},\qquad A=1-\frac{2GM}{rc^2},\qquad B=\left(1-\frac{2GM}{rc^2}\right)^{-1} \tag{B.12}$$

where the conformal function Ω^2 relies on the gravitational potential of the bulk while its influence is inversely proportional to cloud-world potential. In the case of PI18's preferred early Universe positive curvature, the gravitational potential of the bulk can be expressed in terms of the early Universe plasma of mass, M_p, and $\mathfrak{r}$ denoting the radius of curvature of the bulk, where the bulk's potential decreases with the Universe expansion and vanishes in the flat spacetime background $(\mathfrak{r}\to\infty)$. The minus sign of Ω^2 reveals a spatial shrinking through evolving in the conformal time, which agrees with the vortex model that can occur due to the high-speed spinning. By substituting Equations (20) to Equation (8), the conformally metric $\hat{g}_{\mu\nu}=g_{\mu\nu}+2\tilde{g}_{\mu\nu}=g_{\mu\nu}(1+2\Omega^2)$ is
The metric is

$$ds^2=\left(1-\frac{r_s}{r}-\frac{\mathfrak{r}_p}{\mathfrak{r}}\right)\left(-c^2dt^2+S^2\left(\frac{dr^2}{1+\frac{r_s^2}{r^2}-2\frac{r_s}{r}}+\frac{r^2d\theta^2+r^2sin^2\theta d\phi^2}{1-\frac{r_s}{r}-\frac{\mathfrak{r}_p}{\mathfrak{r}}}\right)\right) \tag{B.13}$$

This metric reduces to the Schwarzschild metric in a flat background $(\mathfrak{r}\to\infty)$.

References

[1] Di Valentino E, Melchiorri A and Silk J 2020 Planck evidence for a closed Universe and a possible crisis for cosmology *Nat. Astron.* **4** 196–203

[2] Mokeddem R, Hipólito-Ricaldi W S and Bernui A 2022 Excess of lensing amplitude in the Planck CMB power spectrum *MNRAS* **000**

[3] Handley W 2021 Curvature tension: Evidence for a closed universe *Phys. Rev. D* **103** L041301

[4] Linde A 2003 Can we have inflation with Omega > 1? *J. Cosmol. Astropart. Phys.* **2003** 002–002

[5] Efstathiou G 2003 Is the Low CMB Quadrupole a Signature of Spatial Curvature? *Mon. Not. R. Astron. Soc.* **343** 0–000

[6] Di Valentino E, Mena O, Pan S, Visinelli L, Yang W, Melchiorri A, Mota D F, Riess A G and Silk J 2021 In the realm of the Hubble tension—a review of solutions * *Class. Quantum Gravity* **38** 153001

[7] Riess A G, Filippenko A V., Challis P, Clocchiatti A, Diercks A, Garnavich P M, Gilliland R L, Hogan C J, Jha S, Kirshner R P, Leibundgut B, Phillips M M, Reiss D, Schmidt B P, Schommer R A, Smith R C, Spyromilio J, Stubbs C, Suntzeff N B and Tonry J 1998 Observational Evidence from Supernovae for an Accelerating Universe and a Cosmological Constant *Astron. J.* **116** 1009–38

[8] Brout R, Englert F and Gunzig E 1978 The creation of the universe as a quantum phenomenon *Ann. Phys. (N. Y).* **115** 78–106

[9] Trimble V 2003 Existence and Nature of Dark Matter in the Universe *https://doi.org/10.1146/annurev.aa.25.090187.002233* **25** 425–72

[10] Bull P, Akrami Y, Adamek J, Baker T, Bellini E, Beltrán Jiménez J, Bentivegna E, Camera S, Clesse S, Davis J H, Di Dio E, Enander J, Heavens A, Heisenberg L, Hu B, Llinares C, Maartens R, Mörtsell E, Nadathur S, Noller J, Pasechnik R, Pawlowski M S, Pereira T S, Quartin M, Ricciardone A, Riemer-Sørensen S, Rinaldi M, Sakstein J, Saltas I D, Salzano V, Sawicki I, Solomon A R, Spolyar D, Starkman G D, Steer D, Tereno I, Verde L, Villaescusa-Navarro F, von Strauss M and Winther H A 2016 Beyond ΛCDM: Problems, solutions, and the road ahead *Phys. Dark Universe* **12** 56–99

[11] Sahni V 2002 The Cosmological Constant Problem and Quintessence *Class. Quantum Gravity* **19** 3435–48

[12] Sivanandam N 2013 Is the cosmological coincidence a problem? *Phys. Rev. D - Part. Fields, Gravit. Cosmol.* **87** 083514

[13] Schöneberg N, Lesgourgues J and Hooper D C 2019 The BAO+BBN take on the Hubble tension

[14] Dainotti M G, De Simone B, Schiavone T, Montani G, Rinaldi E and Lambiase G 2021 On the Hubble Constant Tension in the SNe Ia Pantheon Sample *Astrophys. J.* **912** 150

[15] Landau L D 1986 *Theory of Elasticity* (Elsevier)

[16] Al-Fadhli M B 2022 Celestial and Quantum Propagation, Spinning, and Interaction as 4D Relativistic Cloud-Worlds Embedded in a 4D Conformal Bulk: From String to Cloud Theory

[17] Lachì Eze-Rey M and Luminet J-P 2003 COSMIC TOPOLOGY *arXivgr-qc/9605010v2 9 Jan 2003*

[18] Ellis G F R and van Elst H 1998 Cosmological models (Carg\`{e}se lectures 1998)

[19] Straumann N 2013 General Relativity (Graduate Texts in Physics) *Springer* (Springer)

[20] S. M. Carroll 2003 Spacetime and Geometry: An Introduction to General Relativity

[21] M. P. Hobson, Hobson/Efstathiou/Lasenby, G. P. Efstathiou A N L General Relativity - Google Books

[22] Ryden B 2006 *Introduction to Cosmology* (San Francisco, CA, USA: Addison Wesley, ISBN 0-8053-8912-1.)

[23] Aguado D S, Ahumada R, Almeida A, Anderson S F, Andrews B H, Anguiano B, Ortíz E A, Aragón-Salamanca A, Argudo-Fernández M, Aubert M, Avila-Reese V, Badenes C, Rembold S B, Barger K, Barrera-Ballesteros J, Bates D, Bautista J, Beaton R L, Beers T C, Belfiore F, Bernardi M, Bershady M, Beutler F, Bird J, Bizyaev D, Blanc G A, Blanton M R, Blomqvist M, Bolton A S, Boquien M, Borissova J, Bovy J, Brandt W N, Brinkmann J, Brownstein J R, Bundy K, Burgasser A, Byler N, Diaz M C, Cappellari M, Carrera R, Sodi B C, Chen Y, Cherinka B, Choi P D, Chung H, Coffey D, Comerford J M, Comparat J, Covey K, da Silva Ilha G, da Costa L, Dai Y S, Damke G, Darling J, Davies R, Dawson K, de Sainte Agathe V, Machado A D, Moro

 doi:10.20944/preprints202005.0250.v11

A Del, de Lee N, Diamond-Stanic A M, Sánchez H D, Donor J, Drory N, des Bourboux H du M, Duckworth C, Dwelly T, Ebelke G, Emsellem E, Escoffier S, Fernández-Trincado J G, Feuillet D, Fischer J L, Fleming S W, Fraser-McKelvie A, Freischlad G, Frinchaboy P M, Fu H, Galbany L, Garcia-Dias R, García-Hernández D A, Oehmichen L A G, Geimba Maia M A, Gil-Marín H, Grabowski K, Gu M, Guo H, Ha J, Harrington E, Hasselquist S, Hayes C R, Hearty F, Toledo H H, Hicks H, Hogg D W, Holley-Bockelmann K, Holtzman J A, et al 2018 The fifteenth data release of the sloan digital sky surveys: First release of manga derives quantities, data visualization tools and stellar library *arXiv* **55** 23

[24] Kassin S A, Weiner B J, Faber S M, Gardner J P, Willmer C N A, Coil A L, Cooper M C, Devriendt J, Dutton A A, Guhathakurta P, Koo D C, Metevier A J, Noeske K G and Primack J R 2012 THE EPOCH OF DISK SETTLING: z ~ 1 TO NOW *Astrophys. J.* **758** 106

[25] Kassin S A, Brooks A, Governato F, Weiner B J and Gardner J P 2014 *KINEMATIC EVOLUTION OF SIMULATED STAR-FORMING GALAXIES*

[26] Chae K H, Lelli F, Desmond H, McGaugh S S, Li P and Schombert J M 2020 Testing the strong equivalence principle: Detection of the external field effect in rotationally supported galaxies *arXiv* **904** 51

[27] Kroupa P 2012 The dark matter crisis: Falsification of the current standard model of cosmology *Publ. Astron. Soc. Aust.* **29** 395–433

[28] McGaugh S S 2012 The baryonic tully-fisher relation of gas-rich galaxies as a test of ΛcDM and MOND *Astron. J.* **143** 40

[29] Guo Q, Hu H, Zheng Z, Liao S, Du W, Mao S, Jiang L, Wang J, Peng Y, Gao L, Wang J and Wu H 2019 Further evidence for a population of dark-matter-deficient dwarf galaxies *Nat. Astron.* **4** 246–51

[30] van Dokkum P, Danieli S, Abraham R, Conroy C and Romanowsky A J 2019 A Second Galaxy Missing Dark Matter in the NGC 1052 Group *Astrophys. J.* **874** L5

[31] Danieli S, van Dokkum P, Conroy C, Abraham R and Romanowsky A J 2019 Still Missing Dark Matter: KCWI High-resolution Stellar Kinematics of NGC1052-DF2 *Astrophys. J.* **874** L12

[32] Pavel Grinfeld 2013 *Introduction to Tensor Analysis and the Calculus of Moving Surfaces* (Springer)

[33] Dyer E and Hinterbichler K 2009 Boundary terms, variational principles, and higher derivative modified gravity *Phys. Rev. D - Part. Fields, Gravit. Cosmol.* **79**

[34] Krishnan V V, Bailes M, Van Straten W, Wex N, Freire P C C, Keane E F, Tauris T M, Rosado P A, Bhat N D R, Flynn C, Jameson A and Osłowski S 2020 *Lense-Thirring frame dragging induced by a fast-rotating white dwarf in a binary pulsar system*

[35] Feng W-X, Yu H-B and Zhong Y-M 2021 Seeding Supermassive Black Holes with Self-interacting Dark Matter: A Unified Scenario with Baryons *Astrophys. J. Lett.* **914** L26

[36] Shen Y 2009 Supermassive black holes in the hierarchical universe: A general framework and observational tests *Astrophys. J.* **704** 89–108

[37] Snios B, Nulsen P E J, Kraft R P, Cheung C C, Meyer E T, Forman W R, Jones C and Murray S S 2019 *Detection of Superluminal Motion in the X-Ray Jet of M87*

[38] Wang Q D 2021 Chandra large-scale mapping of the Galactic Centre: probing high-energy structures around the central molecular zone *Mon. Not. R. Astron. Soc.* **504** 1609–18

[39] Heywood I, Camilo F, Cotton W D, Yusef-Zadeh F, Abbott D, Adam M, Aldera M A, Bauermeister F, Booth S, Botha A G, Botha D H, Brederode L S, Brits Z B, Buchner S J, Burger J P, Chalmers J M, de Villiers D, Dikgale-Mahlakoana M A, du toit L J, P esterhuyse S W, Fanaroff B L, Foley A, Fourie D J, Gamatham G, Goedhart S, Gounden S, Hlakola M J, Hoek C J, Hokwana A, Horn D M, G Horrell J M, Hugo B, Isaacson A, Jonas J L, B L Jordaan J D, Joubert A F, G Józsa G I, Julie P M, Kapp F B, Kenyon J S, A Kotzé P P, Kriel H, Kusel W, Liebenberg D, Loots A, Lunsky B M, Macfarlane P S, Magnus L G, Magozore C M, Mahgoub O, L Main J P, Malan J A, Malgas D, Manley J, J Maree M D, Merry B, Mnyandu N, Moeng I P, Mphego M C, New W S, Ngcebetsha B, Oozeer N, Otto A J, Passmoor S S, Patel A A, Peens-Hough A, Perkins S J, ratcliffe S

M, rust A, Salie S, Schwardt L C, Serylak M, Sirothia S K, Smirnov O M, Sofeya L, Swart P S, tasse C, taylor D, theron I P, thorat K, tiplady A J, tshongweni S, van Balla J, van der Byl A, van der Merwe C, van Dyk C L, rooyen V, Van tonder V, Wyk V, Wallace B H, Welz M G and Williams L P Inflation of 430-parsec bipolar radio bubbles in the Galactic Centre by an energetic event *Nature*

[40] Reid S, Podolefsky H and Pual A 2013 Fluid Pressure and Flow, PhET Interactive Simulations.

[41] Becerra-Vergara E A, Argüelles C R, Krut A, Rueda J A and Ruffini R 2021 Hinting a dark matter nature of Sgr A* via the S-stars *Mon. Not. R. Astron. Soc. Lett.* **505** L64–8

[42] Burkert A, Schartmann M, Alig C, Gillessen S, Genzel R, Fritz T K and Eisenhauer F 2012 Physics of the galactic center cloud G2, on its way toward the supermassive black hole *Astrophys. J.* **750** 58

[43] Aghanim N, Akrami Y, Ashdown M, Aumont J, Baccigalupi C, Ballardini M, Banday A J, Barreiro R B, Bartolo N, Basak S, Battye R, Benabed K, Bernard J P, Bersanelli M, Bielewicz P, Bock J J, Bond J R, Borrill J, Bouchet F R, Boulanger F, Bucher M, Burigana C, Butler R C, Calabrese E, Cardoso J F, Carron J, Challinor A, Chiang H C, Chluba J, Colombo L P L, Combet C, Contreras D, Crill B P, Cuttaia F, De Bernardis P, De Zotti G, Delabrouille J, Delouis J M, Di Valentino E, Diego J M, Doré O, Douspis M, Ducout A, Dupac X, Dusini S, Efstathiou G, Elsner F, Enßlin T A, Eriksen H K, Fantaye Y, Farhang M, Fergusson J, Fernandez-Cobos R, Finelli F, Forastieri F, Frailis M, Fraisse A A, Franceschi E, Frolov A, Galeotta S, Galli S, Ganga K, Génova-Santos R T, Gerbino M, Ghosh T, González-Nuevo J, Górski K M, Gratton S, Gruppuso A, Gudmundsson J E, Hamann J, Handley W, Hansen F K, Herranz D, Hildebrandt S R, Hivon E, Huang Z, Jaffe A H, Jones W C, Karakci A, Keihänen E, Keskitalo R, Kiiveri K, Kim J, Kisner T S, Knox L, Krachmalnicoff N, Kunz M, Kurki-Suonio H, Lagache G, Lamarre J M, Lasenby A, Lattanzi M, Lawrence C R, Le Jeune M, Lemos P, Lesgourgues J, Levrier F, et al 2020 Planck 2018 results: VI. Cosmological parameters *Astron. Astrophys.* **641**

[44] Ryskin G 2020 Vanishing vacuum energy *Astropart. Phys.* **115** 102387